Therapeutic efficacy of an oral nucleoside analog of remdesivir against SARS-CoV-2 pathogenesis in mice.

Alexandra Schäfer [1, 4], David R. Martinez [1, 4], John J. Won [1], Fernando R. Moreira [1], Ariane J. Brown [1], Kendra L. Gully [1], Rao Kalla [2], Kwon Chun [2], Venice Du Pont [2], Darius Babusis [2], Jennifer Tang [2], Eisuke Murakami [2], Raju Subramanian [2], Kimberly T Barrett [2], Blake J. Bleier [2], Roy Bannister [2], Joy Y. Feng [2], John P. Bilello [2], Tomas Cihlar [2], Richard L. Mackman [2], Stephanie A. Montgomery [3], Ralph S. Baric [1], Timothy P. Sheahan [1, *]

[1] Department of Epidemiology, University of North Carolina at Chapel Hill, Chapel Hill, NC, USA,

[2] Gilead Sciences, Inc, Foster City, CA, USA,

[3] Department of Pathology and Laboratory Medicine, University of North Carolina School of Medicine, Chapel Hill, NC, USA,

[4] These authors contributed equally to this manuscript.

[*] Timothy P. Sheahan. sheahan@email.unc.edu

Abstract

The COVID-19 pandemic remains uncontrolled despite the rapid rollout of safe and effective SARS-CoV-2 vaccines, underscoring the need to develop highly effective antivirals. In the setting of waning immunity from infection and vaccination, breakthrough infections are becoming increasingly common and treatment options remain limited. Additionally, the emergence of SARS-CoV-2 variants of concern with their potential to escape therapeutic monoclonal antibodies emphasizes the need to develop second-generation oral antivirals targeting highly conserved viral proteins that can be rapidly deployed to outpatients. Here, we demonstrate the in vitro antiviral activity and in vivo therapeutic efficacy of GS-621763, an orally bioavailable prodrug of GS-441524, the parental nucleoside of remdesivir, which targets the highly conserved RNA-dependent RNA polymerase. GS-621763 exhibited significant antiviral activity in lung cell lines and two different human primary lung cell culture systems.

35   The dose-proportional pharmacokinetic profile observed after oral administration of GS-621763

36   translated to dose-dependent antiviral activity in mice infected with SARS-CoV-2. Therapeutic

37   GS-621763 significantly reduced viral load, lung pathology, and improved pulmonary function

38   in COVID-19 mouse model. A direct comparison of GS-621763 with molnupiravir, an oral

39   nucleoside analog antiviral currently in human clinical trial, proved both drugs to be similarly

40   efficacious. These data demonstrate that therapy with oral prodrugs of remdesivir can

41   significantly improve outcomes in SARS-CoV-2 infected mice. Thus, GS-621763 supports the

42   exploration of GS-441524 oral prodrugs for the treatment of COVID-19 in humans.

43

44   **Introduction**

45   SARS-CoV-2 emerged in December 2019 and has caused 223 million infections and 4.6

46   million deaths worldwide as of September 2021 (*1-3*). While there are multiple effective

47   vaccines, vaccination rates have lagged in the United States (U.S.) due to vaccine hesitancy and

48   public mistrust thus delaying the generation of herd immunity required to significantly diminish

49   community spread. In addition, outside of the U.S., many countries do not have equitable access

50   to vaccines and/or have been slow to vaccinate (*4-7*). This collective constellation of events is

51   fueling the generation of viral variants that are increasingly transmissible and are ever evolving

52   to escape human immunity. Therefore, there is an immediate unmet need for oral antivirals that

53   can be rapidly disseminated to treat COVID-19 cases in the unvaccinated, the

54   immunocompromised and in vaccine breakthrough cases. Next-generation oral coronavirus

55   (CoV) antivirals, if widely disseminated and given early in infection, could curtail the duration of

56   disease, reduce long-term sequelae of COVID-19, minimize household transmissions, and lessen

57   hospitalizations, thus having a broad impact on public health.

58   There are multiple direct-acting antiviral (DAA) therapies in use to treat COVID-19 (*8-*

59   *12*), including Emergency Use Authorization (EUA)-approved monoclonal antibodies (mAbs)

60   and FDA-approved remdesivir (RDV, GS-5734). Monoclonal antibodies have demonstrated

61   efficacy for treating active COVID-19 cases in outpatients (Regeneron outpatient studies) but

62   currently, all mAbs must be administered via injection, limiting their use to those with ready

63   access to healthcare (*13, 14*). In addition, several SARS-CoV-2 variants of concern (VOCs) have

64   evolved that are resistant to first-line mAb therapies (*15, 16*). Currently, RDV is the only FDA-

65   approved small-molecule direct-acting antiviral to treat COVID-19, but there are several other

66   DAAs currently in human clinical trials including nucleoside analogs molnupiravir (MPV,

67   EIDD-2801) and AT-527, as well as MPro inhibitor PF-07321332 (*17-25*) . Unlike mAbs which

68   specifically target the virion surface exposed spike protein of SARS-CoV-2, nucleoside analog

69   drugs target a highly conserved viral enzyme among CoV, the RNA-dependent RNA polymerase

70   (RdRp) nsp12, rendering them broadly active against multiple emerging, endemic and enzootic

71   CoV. Moreover, due to its high degree of conservation among CoV, the RdRp likely does not

72   have the same capacity for mutational change as spike, which may translate into RdRp having a

73   higher barrier to resistance (*18-20*). Despite demonstrated therapeutic efficacy of RDV against

74   SARS-CoV-2 in animal models (*17, 23, 26*) and in human clinical trials (*8*), the requirement of

75   intravenous administration has limited its widespread use during this pandemic. The orally

76   bioavailable nucleoside prodrug GS-621763, is designed for optimal delivery of the parent

77   nucleoside GS-441524 into systemic circulation, which is then metabolized inside cells into the

78   same active nucleoside triphosphate formed by RDV (*27*). Here, we detail the *in vitro* antiviral

79   activity in various cell models and *in vivo* therapeutic efficacy of oral GS-621763 in a mouse

80   model of SARS-CoV-2 pathogenesis.

81

82   **Results**

83   **GS-621763 has antiviral activity against SARS-CoV-2 in cell lines and human primary cell**

84   **cultures.**

85   GS-441524 is the parental adenosine nucleoside analog (Fig. 1A) of both

86   monophosphoramidate prodrug RDV (GS-5734, Fig. 1B), and triester prodrug GS-621763 (Fig.

87   1C). All three molecules are metabolized to the same active nucleotide triphosphate in cells, but

88   through different activation pathways. GS-621763 is rapidly metabolized during oral absorption

89   to GS-441524, then intracellularly converted by cellular kinases to the analog monophosphate

90   metabolite before further metabolism to the active nucleoside triphosphate. In contrast, the intact

91   phosphoramidate prodrug, RDV, is broken down inside cells directly to the same monophosphate

92   metabolite, effectively bypassing the rate-limiting first phosphorylation step of GS-441524 (*27*).

93   To determine if GS-621763 could inhibit replication of SARS-CoV-2 in cellular assays, we first

94   evaluated its antiviral activity against a SARS-CoV-2 reporter virus expressing nanoluciferase

95   (SARS-CoV-2 nLUC) in A549-hACE2 cells stably expressing the human entry receptor

96   angiotensin-converting enzyme 2 (ACE2) (*28*). With GS-621763, we observed a dose-dependent

97   antiviral effect on SARS-CoV-2 nLUC replication with an average half-maximum effective

98   concentration (EC_{50}) of 2.8 μM (Fig. 1D, Fig.1H, and Supplementary Figure 1A). In the same

99   assay, we measured EC_{50} values for the control compound RDV of 0.28 μM, similar to those

100   reported previously in these cells and reflective of the enhanced ability of the phosphoramidate

101   prodrug to rapidly and efficiently generate active triphosphate by bypassing the slower initial

102   phosphorylation step (Fig. 1D, Fig. 1H, Supplementary Figure 1A) (*29*). As was observed in

103   other cell systems, the parental nucleoside, GS-441524, was less potent (EC_{50} = 3.3 μM) than

104   RDV in our assay and was similar in potency to GS-621763. This suggests that the tri-isobutyryl

105   esters of GS-621763 are efficiently cleaved in the assay to release GS-441524 (Fig. 1D, Fig. 1H,

106   Supplementary Figure 1A). Importantly, we did not observe any measurable cytotoxicity of any

107   of the inhibitors in A549-hACE2 cells at concentrations up to 10 µM (Figure 1F, Supplementary

108   Figure 1B). Human primary airway epithelial (HAE) cell cultures model the cellular complexity

109   and architecture of the human conducting airway and are often used to determine if drugs are

110   transported and metabolized in the cells targeted by emerging CoV in vivo (*18*). In HAE cells

111   infected with WT SARS-CoV-2 (*28*) and treated with GS-621763, we observed a dose-

112   dependent and significant reduction in infectious virus production as compared to DMSO-

113   vehicle treated cultures (Fig. 1F). In similarly infected, control compound (i.e. RDV or GS-

114   441524) treated cultures, a significant and dose-dependent reduction in viral titers was also

115   observed (Fig. 1F). GS-621763, RDV, and GS-441524 inhibited reporter SARS-CoV-2

116   expressing Firefly luciferase (SARS-CoV-2 Fluc) replication in normal human bronchial

117   epithelial (NHBE) cultures with EC_{50} values of 0.125, 0.0371, and 2.454 µM, respectively (Fig.

118   1G, Fig. 1H). All together, these data show that GS-621763 is transported, metabolized and

119   potently antiviral human primary cell systems that model the tissues targeted by SARS-CoV-2 in

120   humans.

121

122   **Dose-dependent therapeutic efficacy of GS-621763 in mouse models of COVID-19 disease.**

123   We have previously performed multiple studies describing the therapeutic efficacy of

124   subcutaneously administered RDV in mice (*Ces1c*^{-/-} C57BL/6J) genetically deleted for a secreted

125   plasma carboxylesterase 1c (*Ces1c*) absent in humans but dramatically reduces drug half-life in

126   wild-type mice (*17-19, 26, 30*).

127   However, the prodrug GS-621763 is designed to be rapidly cleaved pre-systemically in

128   vivo to release GS-441524 into circulation, with no or very minimal intact ester observed in

129   plasma. Therefore, GS-621763 can be studied in wild-type mice where it should also be rapidly

130   converted to parent GS-441524. Plasma pharmacokinetics following a single oral administration

131   of GS-621763 at either 5 or 20 mg/kg were first determined in uninfected BALB/c mice (Fig.

132   2A). Doses were selected to provide high plasma exposures of GS-441524 that would support

133   active triphosphate formation in the lung and to confirm pharmacokinetic dose proportionality

134   needed to project exposures in efficacy studies. Previous studies had shown that parent

135   nucleoside was at least 10-fold less efficient at generating lung triphosphate than RDV, on a

136   molar basis, thus requiring higher plasma exposures of parental GS-441524 to account for the

137   reduced metabolic efficiency (27). No exposure of intact ester prodrug, within the limit of

138   detection, was observed in mice. GS-441524 was both rapidly absorbed and then cleared from

139   systemic circulation, exhibiting a short plasma half-life of approximately 1 hr. Dose

140   proportional increases in both maximal plasma concentrations (C_{max}) and exposures (AUC_{0-24h})

141   at the two doses were observed (Fig. 2A).

142   To better understand the pharmacokinetic and pharmacodynamic relationship for GS-

143   621763, we performed a series of dose-finding studies in BALB/c mice infected with mouse-

144   adapted SARS-CoV-2 (SARS-CoV-2 MA10) (30). In young adult BALB/c mice infected with

145   10^4 plaque forming units (PFU) SARS-CoV-2 MA10, virus replicates to high titers in the

146   respiratory tract, mice lose 15-20% of their body weight by 4 days post-infection (dpi), and acute

147   lung injury/loss of pulmonary function is typically observed after virus replication peaks on 2 dpi

148   (30). We first defined the minimum dosage sufficient for maximal therapeutic efficacy in

149   BALB/c mice initiating twice daily (i.e. bis in die, BID) oral treatment with either vehicle control

150   or 3 mg/kg, 10 mg/kg, or 30 mg/kg GS-621763 beginning 8 hours post infection (hpi) with 10^4

151   PFU SARS-CoV-2 MA10 (Fig. 2B). Unlike vehicle or 3 mg/kg GS-621763 treated animals,

152   mice receiving either 10 or 30 mg/kg GS-621763 were completely protected from weight loss

153   thus demonstrating that early oral antiviral therapy can prevent the progression of disease (Fig.

154   2B). Congruent with the weight loss phenotype, both 10 and 30 mg/kg GS-621763 treated

155   animals had significantly reduced viral lung titers as compared to both the vehicle and 3 mg/kg

156   treated groups (Fig. 2C). To monitor the effect of drug treatment on pulmonary function, we

157   performed daily whole-body plethysmography (WBP) with a subset of mice from each group

158   (N=4 per treatment group). As shown with the WBP metric PenH, whose elevation is associated

159   with airway resistance or obstruction (*18*), we observed a drug dose-dependent reduction in

160   PenH with the maximal effect seen in the 30 mg/kg GS-621763 dose group which was

161   completely protected from the loss of pulmonary function observed in the other treatment groups

162   and vehicle (Fig. 2D). Mice treated with 3 and 10 mg/kg GS-621763 had impaired lung function

163   at days 2 and 3 post infection, but lung function returned to baseline by 4 dpi for all GS-621763

164   treated animals (Fig. 2D). Consistent with weight loss, virus titer, and pulmonary function data,

165   mice treated with 10 or 30 mg/kg had significantly reduced lung congestion, a gross pathologic

166   feature characteristic of severe lung damage (Fig. 2E). We then scored lung tissue sections for

167   the histologic features of acute lung injury (ALI) using two complementary semiquantitative

168   tools. First, using an ALI scoring tool created by the American Thoracic Society (ATS), we

169   blindly evaluated three diseased fields per lung section for several features of ALI including

170   alveolar septal thickening, neutrophils in the interstitium and in air spaces, proteinaceous debris

171   in airspaces, and the presence of hyaline membranes. Only mice treated with 30 mg/kg had

172   significantly reduced ALI scores (Fig. 2F). Second, we used a complementary tool measuring

173   the pathologic hallmark of ALI, diffuse alveolar damage (DAD). Mice in all treated groups

174   showed reduced DAD scores, but only mice receiving 30 mg/kg had significantly decreased

175   DAD in their lungs (Fig. 2G). Together, these data demonstrate that the oral delivery of the

176   nucleoside analog GS-621763 can significantly diminish SARS-CoV-2 virus replication and

177   associated pulmonary disease in a dose-dependent manner.

178

179   **Extended therapeutic protection against COVID-19 disease by GS-621763 in mice**

180   To determine if the potent therapeutic efficacy of GS-621763 observed with early

181   intervention (8 hr after infection) would extend to later times post infection, we designed a

182   therapeutic efficacy study with six arms where we varied both time of oral therapy initiation and

183   dose level in BALB/c mice infected with SARS-CoV-2 MA10 (Fig.3). As done previously, a

184   control group of animals received vehicle twice daily beginning at 12 hours post infection (hpi).

185   The next three arms of the study were dedicated to the 30 mg/kg GS-621763 dose level, with two

186   of the three arms receiving twice daily dosing initiated at either the 12 hpi ("30 mg/kg BID 12

187   hr" group) or the 24 hpi ("30 mg/kg BID 24 hr" group). The third 30 mg/kg arm was designed to

188   determine if dose frequency could be reduced to once daily (quaque die, QD) if initiated early at

189   12 hpi ("30 mg/kg QD 12 hr" group). In the last two arms, we wanted to evaluate if an increased

190   dose of 60 mg/kg given QD beginning at 12 hr or 24 hr ("60 mg/kg QD 12 hr" and "60 mg/kg

191   QD 24 hr" groups) would improve outcomes over the 30 mg/kg groups. Initiation of 30 mg/kg

192   BID therapy at either 12 or 24 hrs offered significant protection from weight loss (Fig. 3A),

193   extending the robust therapeutic phenotype observed for this dose level when initiated at very

194   early times (at 8 hr) (Fig 2). Interestingly, when we decreased the frequency of 30 mg/kg

195   treatment initiated at 12 hr to once daily ("30 mg/kg QD 12 hr" group), we also observed a

196   significant prevention of body weight loss (Fig 3A), thus levels of drug when administered once

197   a day and begun early (at 12 hr) in the course of infection were sufficient to prevent disease

198   progression. Increasing the dose to 60 mg/kg QD initiated at either 12 hr or 24 hr offered similar

199   protection from weight loss observed with vehicle treatment as the 30 mg/kg groups (Fig. 3A).

200   As body weight loss is a crude marker of viral pathogenesis, we next measured multiple

201   virological, physiologic, and pathologic metrics of disease. First, we measured the levels of

202   infectious virus present in lung tissue on 4 dpi. Unlike vehicle-treated animals who harbored an

203   average titer of $5.6x10^4$ PFU per lung lobe, all GS-621763 dose groups significantly reduced the

204   levels of infectious virus in lung tissue with the average titers of most groups falling below the

205   limit of detection (90 PFU). Interestingly, 30 mg/kg delivered QD had significantly elevated

206   viral lung titers (mean titer = $4x10^2$ PFU) as compared to its BID counterpart (mean titer = < 90

207   PFU). A similar trend among treatment groups was observed when measuring the levels of

208   SARS-CoV-2 subgenomic and genomic nucleocapsid (N) RNA in parallel lung tissues (Fig. 3C).

209   All 30 mg/kg groups significantly reduced levels of SARS-CoV-2 RNA in lung tissue as

210   compared to vehicle-treated animals. As observed for infectious titers, 30 mg/kg given QD daily

211   beginning at 12 hr had elevated levels of N RNA as compared to 30 mg/kg given BID beginning

212   at 12 hr suggesting that trough and/or daily exposure levels of drug with QD dosing are

213   insufficient to suppress replication similarly to BID dosing. Increasing the once-daily dose to 60

214   mg/kg to raise the daily exposure and trough levels offered similar reductions in SARS-CoV-2 N

215   RNA as compared to 30 mg/kg BID when initiated at 12 hr, but the levels of viral RNA in the

216   higher dose 60mg/kg group initiated at 24 hr were not different than vehicle (Fig. 3C). Although

217   vehicle-treated animals exhibited significant loss of pulmonary function as measured by WBP,

218   this was largely prevented with GS-621763 therapy (Fig. 3D). All therapy groups initiated at 12

219   hr were equally protected from loss of pulmonary function as measured by the PenH metric (Fig.

220   3D). Of all groups actively receiving GS-621763, animals in the 30 mg/kg BID 24 hr group had

221   a measurable loss of lung function on 3 dpi which resolved by 4 dpi but this phenotype was not

222   extended to other groups. We then scored lung tissue sections for the histologic features of acute

223   lung injury and alveolar damage. Only 30 mg/kg BID initiated at 12 hr significantly reduced ALI

224   scores as compared to those in vehicle-treated animals. In addition, the 30 mg/kg BID 12 hr-

225   group had significantly lower ALI scores as compared to the 60 mg/kg QD 24 hr-group (Figure

226   3E). Only 30 mg/kg given twice a day at 12 hr most dramatically reduced DAD scores but this

227   protection from lung pathology was lost if given once per day or if initiated at 24 hr (Fig. 3G).

228   The high dose of 60 mg/kg QD when initiated at 12 hr improved DAD scores as compared to

229   similarly treated animals that began treatment at 24 hr. Collectively, these data demonstrate that

230   GS-621763 therapy can improve both virologic and pathogenic metrics, but the degree of

231   improvement was dependent on time of initiation and dose frequency.

232

233   **The therapeutic efficacy of GS-621763 is similar to molnupiravir (MPV, EIDD-2801)**

234   MPV is an oral nucleoside analog prodrug antiviral currently in Phase 3 clinical trial to

235   treat COVID-19 with demonstrated antiviral efficacy in mice against several emerging CoV

236   including SARS-CoV, MERS-CoV, and SARS-CoV-2 (*18, 19, 21, 22*). Like GS-621763, MPV

237   is a prodrug which is metabolized in vivo into a parental nucleoside (β-D-N4-hydroxycytidine,

238   NHC) in its metabolic progression towards the antiviral active triphosphate (*20*). To determine if

239   GS-621763 would provide similar protection as MPV, we then designed comparative therapeutic

240   efficacy studies in the mouse model of SARS-CoV-2 pathogenesis described above. Pre-efficacy

241   pharmacokinetic studies in BALB/c mice (30 mg/kg or 100 mg/kg) were performed with MPV

242   and showed dose proportional increases in NHC plasma exposures (Supplemental Fig. 2).

243   Pharmacokinetic modeling then determined that a daily 120 mg/kg dose (given 60 mg/kg BID)

244   would result in exposures similar to that observed in humans receiving 800 mg BID, a dose

245   being evaluated in a human clinical trial (22). The comparative efficacy study included a vehicle

246   group and 5 additional groups receiving two doses of MPV or GS-621763 per day 12 hrs apart

247   (BID). Three arms of the study began dosing at 12 hr: 30 mg/kg GS-621763, 30 mg/kg MPV

248   (0.5× human equivalent dose) or 60 mg/kg MPV (1× human equivalent dose). At 24 hr, we

249   began dosing of two additional groups: 60 mg/kg GS-621763 or 60 mg/kg MPV. While SARS-

250   CoV-2 MA10 infection caused rapid weight loss in vehicle control animals, all animals receiving

251   either GS-621763 or MPV beginning at either 12 or 24 hr were protected from weight loss (Fig.

252   4A). Similarly, upon titration of lung tissues at 4 dpi for infectious virus by plaque assay,

253   vehicle-treated animals had expectedly high levels of infectious virus which was significantly

254   reduced in all treatment groups, independent of drug type or initiation time (Fig. 4B). When

255   treatment was initiated at 12 hr, a moderate yet significant elevation in infectious titers was

256   observed in the 30mg/kg MPV group, inferior to either equivalently dosed GS-621763 animals

257   or those receiving the higher dose (60 mg/kg) of MPV (Fig. 4B). To understand the relationship

258   between levels of infectious virus and viral RNA in lung tissue, we performed qRT-PCR on total

259   RNA for SARS-CoV2 N RNA in parallel tissues utilized for plaque assay. The trend observed

260   with infectious virus is mirrored in the qRT-PCR data where all groups receiving antiviral

261   therapy had significantly reduced levels of viral RNA (Fig. 4C). In addition, animals receiving

262   30 mg/kg MPV (0.5× human equivalent dose) had a measurable increase in N RNA as compared

263   to equivalently dosed GS-621763 animals. Similar to weight loss data, vehicle-treated animals

264   had a significant loss of pulmonary function as measured by WBP on both 3 and 4 dpi which was

265   prevented in all groups receiving antiviral treatment (Fig. 4D). We then blindly evaluated lung

266   tissue sections for the pathological manifestations of ALI and DAD using two complementary

267   histologic tools described above. Congruent with the above data, ALI scores in all antiviral

268   therapy groups were significantly reduced as compared to vehicle controls (Fig. 4E). In

269   agreement with ALI scores, the DAD histologic scores were similarly reduced in all antiviral

270   therapy treated groups as compared to those treated with vehicle (Fig. 4F). All together, these

271   data show that antiviral therapy with GS-621763 and MPV when initiated early or at the peak of

272   virus replication (~24 hr) can both significantly diminish virus replication and improve disease

273   outcomes.

274

275   **Discussion**

276   Three novel human CoVs have emerged in the past 20 years, first with SARS-CoV in

277   2002-2003, MERS-CoV in 2012 and most recently, SARS-CoV-2 in 2019 (*1, 2, 31*). Vaccine

278   availability, vaccine hesitancy, and the ongoing evolution and emergence of VOCs are

279   collectively delaying the global control of pandemics and potential achievement of global herd

280   immunity and may prevent it altogether (*15, 32-34*). As such, there is an acute need for broad-

281   spectrum antivirals to treat COVID-19 in the unvaccinated as well as increasingly common

282   breakthrough infections in those vaccinated, driven by immune evading VOCs. In addition, due

283   to the emergence potential of the CoV family, we must also actively develop broadly acting

284   therapies effective the CoVs of today to prepare for those that may emerge in the future. Both

285   RDV and MPV are examples of nucleoside analogs with broad activity against genetically

286   diverse CoV (*35*). Here, we show that GS-621763, a prodrug that improves the oral delivery of

287   parent nucleoside GS-441524, is yet another example of an orally bioavailable nucleoside analog

288   prodrug that is effective against SARS-CoV-2.

289   Oral broadly acting antiviral therapies that target conserved viral proteins with a

290   diminished capacity for evolutionary change will maximize therapeutic utility against future

291   emerging CoV. SARS-CoV-2 has undergone a considerable amount of genetic evolution since

292   its emergence in 2019; each time a globally dominant SARS-CoV-2 VOC has emerged, it has

293   been replaced by a new VOC harboring more concerning characteristics like replicative capacity

294   or transmissibility (*36*). The majority of genetic changes have been localized to viral proteins

295   decorating the surface of the virus particle like the viral spike which has mutated to eradicate

296   epitopes targeted by early and promising monoclonal antiviral therapies (e.g. Eli Lily,

297   Regeneron) rendering them less active against newer VOCs (*37*). Approved antivirals like RDV,

298   those in clinical trials like MPV, AT-527, and PF-07321332 (Pfizer, oral protease inhibitor)

299   target highly conserved enzymes required for virus replication which likely have a diminished

300   capacity for change as compared to the spike protein (*38*). The widespread use of both RDV and

301   mAb therapies in the U.S. and globally has been limited by the necessity of delivery by

302   intravenous infusion which in turn requires access to qualified health care staff and facilities.

303   Thus, effective oral antiviral therapy or combination therapies which can be procured at a

304   pharmacy and self-administered by the patient would help facilitate wide-spread global access

305   and could have profound positive impacts on global public health.

306   In this study, we utilized a mouse adapted SARS-CoV-2 variant, SARS-CoV-2 MA10, in

307   wild-type BALB/c mice. (*17, 30*). Mice infected with this virus develop severe lung disease

308   reminiscent of that seen with severe COVID-19 including the development of ALI and

309   respiratory failure (*30*). It is important to note that the disease resulting from SARS-CoV-2

310   MA10 infection in mice is compressed as compared to that observed in humans with virus titer

311   peaking in the mouse lung between 24-48 hrs after infection, rapid loss of pulmonary function

312   beginning 2-3 dpi, rapid weight loss within the first 4 days of infection, lung pathology

313   consistent with ALI peaking 4-6 dpi and virus induced mortality within a week of infection. This

314   is markedly different than the COVID-19 in humans where virus titers peak in the upper airway

315   within the first week, but viral RNA shedding can be observed for as long as 24 days and

316   symptoms can take weeks to months to resolve (*39-41*). Because of this caveat associated with

317   our mouse model, the time in which to intervene with a direct acting antiviral and sufficiently

318   improve outcomes is curtailed in mice as compared to humans. Our recent study with RDV

319   exemplifies this where we found the degree of therapeutic benefit in mice infected with SARS-

320   CoV-2 MA10 was dependent on the time of initiation (*17*). Here, we show that oral

321   administration with GS-621763 prevents body weight loss, loss of pulmonary function, severe

322   lung pathology and virus replication when administered at 12 and 24 hrs after infection. While

323   we observed improvement in some metrics with RDV initiated at 24 hr in our prior studies (*17*),

324   GS-621763 therapy initiated at a similar time comparatively improved all metrics assessed.

325   Thus, herein we provide proof-of-concept preclinical data that the orally bioavailable ester

326   analog of RDV GS-621763 can exert potent antiviral effects in vivo during an ongoing SARS-

327   CoV-2 infection. Lastly, we show that GS-621763 therapy provides similar levels of protection

328   from SARS-CoV-2 pathogenesis as MPV, an oral nucleoside analog prodrug effective against

329   SARS-CoV-2 in mice that is currently in human clinical trials. Future directions are focused on

330   extending these studies to evaluate the efficacy of combinations of antivirals in our models of

331   SARS-CoV-2 pathogenesis and in other models that can evaluate the blockade of transmission

332   such as hamster and ferret.

333   In summary, we provide preclinical data demonstrating the in vitro antiviral activity and

334   in vivo therapeutic efficacy of an orally bioavailable nucleoside analog prodrug, GS-621763. The

335   data provided herein supports the future evaluation of orally bioavailable prodrugs of GS-441524

336   in humans with COVID-19. If safe and effective, this class of RdRp inhibitors could become part

337   of the arsenal of existing oral antivirals that are desperately needed to address a global unmet

338   need for the COVID-19 pandemic and CoV pandemics of the future.

339

340   **Figure Legends**

341   **Figure 1. Chemical Structure and in vitro potency of GS-621763 in comparison to RDV**

342   **(GS-5734) and GS-441524.**

343   (A) Chemical structure of the parental adenosine nucleoside analog GS-441524.

344   (B) Chemical structure of the monophosphoramidate prodrug RDV.

345   (C) Chemical structure of GS-621763, the tri-isobutyryl ester of GS-441524.

346   (D) Mean percent inhibition of SARS-CoV-2 replication by GS-621763, in comparison to the

347   prodrug RDV - and the parental nucleoside GS-441524 in A459-hACE2 cells (done in

348   triplicates).

349   (E) Cytotoxicity in A459-hACE2 cells treated with GS-621763, RDV, and GS-441524 in A459-

350   hACE2 cells (done in triplicates, CellTiter-Glo – CTG).

351   (F) Inhibition of SARS-CoV-2 replication by GS-621763, in comparison to the prodrug RDV

352   and the parental nucleoside GS-441524 in human primary airway epithelial cells (HAE, done in

353   duplicates).

354   (G) Inhibition of SARS-CoV-2-Fluc replication by GS-621763, RDV -, and the parental

355   nucleoside GS-441524 in normal human bronchial epithelial (NHBE) cultures (done in

356   duplicates).

357   (H) In vitro EC_{50} values for inhibition of viral replication by GS-621763, RDV, and the parental

358   nucleoside GS-441524 in A459-hACE2 and NHBE cells.

359

360   **Figure 2. Dose-dependent therapeutic protection against COVID-19 disease by GS-621763**

361   **in mice.**

362   (A) Plasma Pharmacokinetics of GS-441524 in uninfected Balb/c mice following a single oral

363   administration of GS-621763 at either 5 or 20 mg/kg. Plasma concentrations of GS-621763 were

364   below the limit of quantification at all time points.

365   (B) Depicted is the % starting weight in therapeutically treated mice with vehicle (n=19) or 3

366   mg/kg (n=9), 10 mg/kg (n=10), and 30 mg/kg (n=10) GS-621763 at 8 hr. All mice were infected

367   with $1x10^4$ PFU SARS-CoV-2 MA10.

368   (C) Lung viral titers in therapeutically treated mice with vehicle (n=19) or 3 mg/kg (n=9), 10

369   mg/kg (n=10), and 30 mg/kg (n=10) GS-621763 at 8 hr. All mice were infected with $1x10^4$ PFU

370   SARS-CoV-2 MA10. Limit of detection (LoD)

371   (D) Pulmonary function in therapeutically treated mice with vehicle (n=4) or 3 mg/kg (n=4), 10

372   mg/kg (n=4), and 30 mg/kg (n=4) GS-621763 at 8 hr. All mice were infected with $1x10^4$ PFU

373   SARS-CoV-2 MA10.

374   (E) Lung congestion score in therapeutically treated mice with vehicle (n=19) or 3 mg/kg (n=9),

375   10 mg/kg (n=10), and 30 mg/kg (n=10) GS-621763 at 8 hr. All mice were infected with $1x10^4$

376   PFU SARS-CoV-2 MA10.

377   (F and G) Lung pathology in the therapeutically treated mice with vehicle (n=19) or 3 mg/kg

378   (n=9), 10 mg/kg (n=10), and 30 mg/kg (n=10) GS-621763 at 8 hr. All mice were infected with

379   1×10^4 PFU SARS-CoV-2 MA10.

380   Data were analyzed using two-way ANOVA (weight loss and lung function) and Kruskal-Wallis

381   test (lung titer, congestion score, and pathology scores), *$p < 0.05$, **$p < 0.005$, ***$p < 0.0005$,

382   ****$p < 0.0001$

383

384   **Figure 3. Extended therapeutic protection of mice against COVID-19 disease by oral GS-**

385   **621763 in mice.**

386   (A) Depicted is the % starting weight in therapeutically treated mice with either 30 mg/kg or 60

387   mg/kg BID or QD GS-621763 at 12 and 24 hrs (n=10 for all treatment groups, except n=8 for 60

388   mg/kg, 12 hr QD treatment group). All mice were infected with 1×10^4 PFU SARS-CoV-2

389   MA10.

390   (B) Lung viral titers in therapeutically treated mice with either 30 mg/kg or 60 mg/kg BID or QD

391   GS-621763 at 12 and 24hrs (n=10 for all treatment groups, except n=8 for 60 mg/kg, 12 hr QD

392   treatment group). All mice were infected with 1×10^4 PFU SARS-CoV-2 MA10. Limit of

393   detection (LoD).

394   (C) Viral N RNA in therapeutically treated mice with either 30 mg/kg or 60 mg/kg BID or QD

395   GS-621763 at 12 and 24 hrs (n=10 for all treatment groups, except n=8 for 60 mg/kg, 12 hr QD

396   treatment group). All mice were infected with 1×10^4 PFU SARS-CoV-2 MA10.

397   (D) Pulmonary function in therapeutically treated mice with either 30 mg/kg or 60 mg/kg BID or

398   QD GS-621763 at 12 and 24 hrs (n=4 for all treatment groups). All mice were infected with

399   1×10^4 PFU SARS-CoV-2 MA10.

400   (n=4 for all treatment groups).

401   (F and G) Lung pathology in the therapeutically treated mice with either 30 mg/kg or 60 mg/kg

402   BID or QD GS-621763 at 12 and 24 hrs (n=10 for all treatment groups, except n=8 for 60 mg/kg,

403   12 hr QD treatment group, and n=7 for vehicle group).

404   Data were analyzed using two-way ANOVA (weight loss and lung function) and Kruskal-Wallis

405   test (lung titer, lung viral RNA, and pathology scores), $*p<0.05$, $**p<0.005$, $***p<0.0005$,

406    $****p<0.0001$.

407

408   **Figure 4. Evaluation of therapeutic intervention of GS-621763 in comparison to**

409   **molnupiravir (MPV).**

410   (A) Depicted is the % starting weight in therapeutically treated mice with either 30 mg/kg or 60

411   mg/kg GS-621763 or MPV at 12 or 24 hrs (n=10 for all treatment groups). All mice were

412   infected with $1x10^4$ PFU SARS-CoV-2 MA10.

413   (B) Lung viral titers in therapeutically treated mice with either 30 mg/kg or 60 mg/kg GS-

414   621763 or MPV at 12 or 24 hrs (n=10 for all treatment groups). All mice were infected with

415    $1x10^4$ PFU SARS-CoV-2 MA10. Limit of detection (LoD).

416   (C) Viral N RNA in therapeutically treated mice with either 30 mg/kg or 60 mg/kg GS-621763

417   or MPV at 12 or 24 hrs (n=10 for all treatment groups). All mice were infected with $1x10^4$ PFU

418   SARS-CoV-2 MA10.

419   (D) Pulmonary function in therapeutically treated mice with either 30 mg/kg or 60mg/kg GS-

420   621763 or MPV at 12 or 24 hrs (n=4 for all treatment groups). All mice were infected with $1x10^4$

421   PFU SARS-CoV-2 MA10.

422 (F and G) Lung pathology in the therapeutically treated mice with either 30 mg/kg or 60 mg/kg

423 GS-621763 or MPV at 12or 24 hrs (n=10 for all treatment groups). All mice were infected with

424 $1x10^4$ PFU SARS-CoV-2 MA10.

425 Data were analyzed using two-way ANOVA (weight loss and lung function) and Kruskal-Wallis

426 test (lung titer, lung viral RNA, and pathology scores), $*p<0.05$, $**p<0.005$, $***p<0.0005$,

427 $****p<0.0001$

428

429 **Supplemental Figure 1. In vitro potency and toxicity of GS-621763, RDV, and GS-441524**

430 **in A549-hACE2 cells**

431 (A) Raw data for the inhibition of SARS-CoV-2 replication by GS-621763, RDV, and GS-

432 441521 in A459-hACE2 cells measured through quantitation of SARS-CoV-2 expressed nano

433 luciferase (nLuc), measured in triplicates.

434 (B) Raw data for cytotoxicity in A459-hACE2 cells treated with GS-621763, RDV, and GS-

435 441521 in A459-hACE2 cells measured via CellTiter-Glo, (measured in triplicates).

436 C) Raw data for the inhibition of SARS-CoV-2-Fluc replication by GS-621763, RDV, and GS-

437 441521 in NHBE cultures measured through quantitation of SARS-CoV-2 expressed firefly

438 luciferase (Fluc), measured in duplicates, repeated twice.

439

440 **Supplemental Figure 2. Molnupiravir mouse plasma pharmacokinetics**

441 Plasma Pharmacokinetics of N-hydroxycytidine (NHC) in uninfected Balb/c mice following

442 daily oral administration of molnupiravir at either 60 or 200 mg/kg (as either 30 or 100

443 mg/kg/dose given BID; molnupiravir at all timepoints).

444

445   **Material and Methods**

446   **Small molecule drug synthesis and formulation**

447   GS-621763, RDV, and GS-441524 were synthesized at Gilead Sciences Inc., and their chemical

448   identity and purity were determined by nuclear magnetic resonance, and high-performance

449   liquid chromatography (HPLC) analysis (*27*). Molnupiravir was purchased from

450   MedChemExpress LLC (NJ, USA) with a purity of 95% based on HPLC analysis.

451   Small molecules were solubilized in 100% DMSO for in vitro studies and in vehicle

452   containing 2.5% DMSO; 10% Kolliphor HS-15; 10% Labrasol; 2.5% Propylene glycol; 75%

453   Water (final formulation pH 2) (for GS-621763) and in vehicle containing 2.5% Kolliphor RH-

454   40, 10% Polyethylene glycol 300, 87.5% Water (for MPV) for in vivo studies. GS-621763, GS-

455   441524, GS-5734 were made available to the University of North Carolina (UNC) at Chapel Hill

456   under a materials transfer agreement with Gilead Sciences.

457

458   **In vivo plasma pharmacokinetic analysis of GS-621763 and molnupiravir (MPV)**

459   Mice were orally administered either a single dose of GS-621763 (in vehicle containing

460   2.5% DMSO; 10% Kolliphor HS-15; 10% Labrasol; 2.5% Propylene glycol; 75% Water (final

461   formulation pH 2) or two doses of molnupiravir (in vehicle containing 2.5% Kolliphor RH-40,

462   10% Polyethylene glycol 300, 87.5% Water) (BID, 12 hours apart). GS-621763 was given at

463   either 5 or 20 mg/kg and MPV at either 30 or 100 mg/kg. Plasma was serially isolated from 4

464   mice at 0.25, 1, 2, 8 and 24 hrs post GS-621763 administration. Plasma was isolated from

465   alternating groups of 4 mice per timepoint at 0.5, 2, 6, 12 (pre-second dose), 12.5, 18 and 24

466   hrs post MPV administration. 20 µl of plasma was added to a mixture containing 250 µl of

467   methanol and 25 µL of internal standard solution and centrifuged. 250 µl of resulting

468   supernatant was then transferred, filtered (Agilent Captiva 96, 0.2 μm) and dried under a stream

469   of nitrogen at 40 ºC. Following reconstitution in a mixture of 5% acetonitrile and 95% water, a

470   10 μl aliquot was injected onto an LC-MS/MS system. Plasma concentrations of either GS-

471   621763 and GS-441524 or MPV and N-hydroxycytidine (NHC) were determined using 8 to 10-

472   point calibration curves spanning at least 3 orders of magnitude with quality control samples to

473   ensure accuracy and precision, prepared in normal mouse plasma. Analytes were separated by a

474   50 mm × 3.0 mm, 2.55 μm Synergi Polar-RP column (Phenomenex) using a multi-stage linear

475   gradient from 5% to 95% acetonitrile in mobile phase A at a flow rate of 1 ml/min.

476

477   **Quantitation of GS-441524 metabolites in the lung following oral GS-621763**

478   **administration in *Balb/c* mice**

479   Lungs from all mice administered GS-621763 were quickly isolated at 24 hrs post-dose

480   and immediately snap frozen in liquid nitrogen. On dry ice, frozen lung samples were

481   pulverized and weighed. Dry ice-cold extraction buffer containing 0.1% potassium hydroxide

482   and 67 mM ethylenediamine tetraacetic acid (EDTA) in 70% methanol, containing 0.5μM

483   chloro-adenosine triphosphate as internal standard was added and homogenized. After

484   centrifugation at 20,000 × g for 20 minutes, supernatants were transferred and dried in a

485   centrifuging evaporator. Dried samples were then reconstituted with 60 μL of mobile phase A,

486   containing 3 mM ammonium formate (pH 5) with 10 mM dimethylhexylamine (DMH) in

487   water, centrifuged at 20,000 × g for 20 minutes and final supernatants transferred to HPLC

488   injection vials. An aliquot of 10 μl was subsequently injected onto an API 6500 LC/MS/MS

489   system for analysis of GS-441524 and its phosphorylated metabolites, performed using a

490   similar method as described previously (*18*).

491

Viruses and plaque assay

493 Recombinant SARS-CoV-2 MA10 virus was generated as described previously (*30*). For

494 virus titration by plaque assay, the caudal lobe of the right lung was homogenized in PBS, and

495 the resulting homogenate was serial-diluted and inoculated onto confluent monolayers of Vero

496 E6 cells, followed by agarose overlay. Plaques were visualized with overlay of neutral red dye

497 on day 3 after infection (*30*).

498

In vitro assays for antiviral activity

500 A549-hACE2 cells were plated at a density of 20,000 cells/well/100 µl in black-walled

501 clear-bottom 96-well plates 24 hrs prior to infection. Compounds GS-621763, GS-5734, GS-

502 441524, were diluted in 100% DMSO (1:3) resulting in a 1000X dose response from 10 to 0.002

503 mM (10 to 0.002 µM final). All conditions were performed in triplicate. At BSL3, medium was

504 removed, and cells were infected with 100 µl SARS-CoV-2 nLUC (MOI 0.008) for 1 h at 37 ˚C

505 after which virus was removed, wells were washed (150 µl) with infection media (DMEM, 4%

506 FBS, 1X antibiotic/antimycotic) and infection media (100 µl) containing a dose response of drug

507 was added. Plates were incubated at 37 ˚C for 48 hrs. NanoGlo assay was performed 48 hpi.

508 Sister plates were exposed to drug but not infected to gauge cytotoxicity via CellTiter-Glo assay

509 (CTG, Promega, Madison, WI), 48 hrs post treatment.

510 Normal human bronchial epithelial (NHBE) cells (donor 41219) were purchased from

511 Lonza (Walkersville, MD Cat# CC-2540) and maintained in Bronchial Epithelial Cell Growth

512 Medium (BEGM) (Lonza, Walkersville, MD, Cat# CC-3170) with all provided supplements in

513 the BulletKit. Cells are passaged 2-3 times per week to maintain sub-confluent densities and are

514   used for experiments at passages 2-4. NHBE cells were seeded in 24-well plates at 1×10^5 cells in

515   a final volume of 0.5 ml BEGM^{TM} Bronchial Epithelial Cell Growth Medium (BulletKit^{TM};

516   Lonza, Basel, SW). Cultures were incubated overnight 37 °C with 5% CO_2. On the following

517   day, media was replaced with 0.5 ml growth medium. Cultures were treated with 1:3 serial

518   dilutions of compound using the HP D300e digital dispenser with normalization to the highest

519   concentration of DMSO in all wells (<1% final volume). The cells were then infected with 0.1

520   ml SARS-CoV-2-Fluc diluted in BEGM media at MOI = 5. Uninfected and untreated wells were

521   included as controls to determine compound efficacy against SARS-CoV-2-Fluc. Following

522   incubation with compound and virus for 24 hrs at 37 °C with 5% CO_2, culture supernatant was

523   removed from each well and replaced with 0.3 ml of ONE-Glo luciferase reagent (Promega,

524   Madison, WI). The plates were shaken at 400 rpm for 10 min at room temperature. 0.2 ml of

525   supernatant from each well was transferred to a 96-well opaque plate (Corning) and

526   luminescence signal was measured using an EnVision plate reader (PerkinElmer). Values were

527   normalized to the uninfected and infected DMSO controls (0% and 100% infection,

528   respectively). Data was fit using a four-parameter non-linear regression analysis using Graphpad

529   Prism. EC_{50} values were then determined as the concentration reducing the firefly luciferase

530   signal by 50%. The compiled data was generated based on least two independent experimental

531   replicates, each containing four technical replicates for each concentration.

532   **Mouse studies and in vivo infections**

533   　　All mouse studies were performed at the University of North Carolina (Animal Welfare

534   Assurance #A3410-01) using protocols (#20-059) approved by the University of North Carolina

535   Institutional Animal Care and Use Committee. All animal work was approved by the

536   Institutional Animal Care and Use Committee at University of North Carolina at Chapel Hill

537   according to guidelines outlined by the Association for the Assessment and Accreditation of

538   Laboratory Animal Care and the US Department of Agriculture. All work was performed with

539   approved standard operating procedures and safety conditions for SARS-CoV-2. Our

540   institutional BSL3 facilities are designed to conform to the safety requirements recommended by

541   Biosafety in Microbiological and Biomedical Laboratories, the US Department of Health and

542   Human Services, the Public Health Service, the Centers for Disease Control and Prevention, and

543   the National Institutes of Health. Laboratory safety plans have been submitted, and the facility

544   has been approved for use by the University of North Carolina Department of Environmental

545   Health and Safety and the Centers for Disease Control and Prevention.

546   Even groups (n=10, or less as indicated) of 10-week-old female BALB/c mice (Envigo;

547   #047) were used in all in vivo efficacy studies. For infection, mice were anesthetized with a

548   mixture of ketamine/xylazine and infected with 10^4 PFU of SARS-CoV-2 MA10 in 50 µl PBS

549   intranasally. Vehicle or GS-621673 was administered orally at the dosages and timepoints as

550   indicated. Mice were monitored daily for body weight changes and for lung function by whole-

551   body plethysmography. At 4 dpi, mice were euthanized, and lung tissue was harvested for viral

552   titer analysis, RNA and histology, and lung congestion scores were estimated (*30*). Samples for

553   viral load determination and for RNA isolation were stored at −80 °C until used; histology

554   samples were inactivated in 10% NBF and stored at 4 °C until further processing.

555

556   **Histology and lung pathology scoring**

557   Two separate lung pathology scoring scales, Matute-Bello and Diffuse Alveolar Damage

558   (DAD), were used to quantify acute lung injury (ALI) (*19*).

559   For Matute-Bello scoring samples were blinded and three random fields of lung tissue

560   were chosen and scored for the following: (A) neutrophils in alveolar space (none = 0, 1–5 cells =

561   1, > 5 cells = 2), (B) neutrophils in interstitial space (none = 0, 1–5 cells = 1, > 5 cells = 2), (C)

562   hyaline membranes (none = 0, one membrane = 1, > 1 membrane = 2), (D) Proteinaceous debris

563   in air spaces (none = 0, one instance = 1, > 1 instance = 2), (E) alveolar septal thickening (< 2Å~

564   mock thickness = 0, 2–4Å~ mock thickness = 1, > 4Å~ mock thickness = 2). Scores from A–E

565   were put into the following formula score = [(20x A) + (14 x B) + (7 x C) + (7 x D) + (2 x E)]/100

566   to obtain a lung injury score per field and then averaged for the final score for that sample.

567   In a similar way, for DAD scoring, three random fields of lung tissue were scored for the

568   in a blinded manner for: 1= absence of cellular sloughing and necrosis, 2= uncommon solitary cell

569   sloughing and necrosis (1–2 foci/field), 3=multifocal (3+foci) cellular sloughing and necrosis with

570   uncommon septal wall hyalinization, or 4=multifocal (>75% of field) cellular sloughing and

571   necrosis with common and/or prominent hyaline membranes. To obtain the final DAD score per

572   mouse, the scores for the three fields per mouse were averaged.

573   **RNA isolation and RT-qPCR**

574   Mouse tissue from SARS-CoV-2 infected mice was homogenized using glass beads in

575   TRIzol Reagent (Invitrogen). Equal volume of 100% EtOH was mixed with the TRIzol

576   homogenate and processed using Direct-Zol RNA MiniPrep Kit (Zymo) to extract viral RNA.

577   Optional DNase I treatment was conducted to ensure the adequate removal of unwanted DNA.

578   Eluted RNA was coupled with TaqMan Fast Virus 1-step Master Mix (Applied Biosystems) and

579   nCOV_N1 primers/probe (IDT) to quantify viral load via reverse transcription – quantitative

580   polymerase chain reaction (RT-qPCR). Samples were plated on a MicroAmp EnduraPlate

581   (Applied Biosystems) and run using a QuantStudio 6 Real-Time PCR System (Applied

582   Biosystems) to obtain viral titers. The following PCR program was run: 50 °C for 5 minutes, 95

583   °C for 20 seconds, followed by 45 cycles of 95 °C for 3 seconds and 60°C for 30 seconds. The

584   sequences of the 2019-nCOV_N1 primers and probe were as follows: Forward primer: GAC

585   CCC AAA ATC AGC GAA AT, Reverse primer: TCT GGT TAC TGC CAG TTG AAT CTG,

586   Probe: AC CCC GCA TT ACG TTT GGT GGA CC (CDC N1 qRT-PCR assay (*42*)). SARS-

587   CoV-2 standard curve RNA was produced by PCR amplification of SARS-CoV-2 nucleocapsid

588   by which a 5' T7 polymerase promoter was introduced. This amplicon was used as template to

589   generate in vitro transcribed RNA which was then quantified and serially diluted ($10^8 – 10^1$

590   copies/µl).

602

603   **Competing interest**

604   These authors are employees of Gilead Sciences and hold stock in Gilead Sciences: Rao Kalla,

605   Kwon Chun, Venice Du Pont, Darius Babusis, Jennifer Tang, Eisuke Murakami, Raju

606   Subramanian, Kimberly T Barrett, Blake J. Bleier, Roy Bannister, Joy Y. Feng, John P. Bilello,

607   Tomas Cihlar, and Richard L. Mackman

608

609   **Literature**

610   1.   P. Zhou, X. L. Yang, X. G. Wang, B. Hu, L. Zhang, W. Zhang, H. R. Si, Y. Zhu, B. Li,
611   C. L. Huang, H. D. Chen, J. Chen, Y. Luo, H. Guo, R. D. Jiang, M. Q. Liu, Y. Chen, X.
612   R. Shen, X. Wang, X. S. Zheng, K. Zhao, Q. J. Chen, F. Deng, L. L. Liu, B. Yan, F. X.
613   Zhan, Y. Y. Wang, G. F. Xiao, Z. L. Shi, A pneumonia outbreak associated with a new
614   coronavirus of probable bat origin. *Nature* **579**, 270-273 (2020).
615   2.   N. Zhu, D. Zhang, W. Wang, X. Li, B. Yang, J. Song, X. Zhao, B. Huang, W. Shi, R. Lu,
616   P. Niu, F. Zhan, X. Ma, D. Wang, W. Xu, G. Wu, G. F. Gao, W. Tan, I. China Novel
617   Coronavirus, T. Research, A Novel Coronavirus from Patients with Pneumonia in China,
618   2019. *N Engl J Med* **382**, 727-733 (2020).
619   3.   J. H. University. (2020).
620   4.   A. Binagwaho, K. Mathewos, S. Davis, Time for the ethical management of COVID-19
621   vaccines. *Lancet Glob Health*, (2021).
622   5.   E. Aryeetey, E. Engebretsen, A. Gornitzka, P. Maassen, S. Stolen, A step backwards in
623   the fight against global vaccine inequities. *Lancet* **397**, 23-24 (2021).
624   6.   A. Asundi, C. O'Leary, N. Bhadelia, Global COVID-19 vaccine inequity: The scope, the
625   impact, and the challenges. *Cell Host Microbe* **29**, 1036-1039 (2021).
626   7.   J. R. Barrett, S. Belij-Rammerstorfer, C. Dold, K. J. Ewer, P. M. Folegatti, C. Gilbride,
627   R. Halkerston, J. Hill, D. Jenkin, L. Stockdale, M. K. Verheul, P. K. Aley, B. Angus, D.
628   Bellamy, E. Berrie, S. Bibi, M. Bittaye, M. W. Carroll, B. Cavell, E. A. Clutterbuck, N.
629   Edwards, A. Flaxman, M. Fuskova, A. Gorringe, B. Hallis, S. Kerridge, A. M. Lawrie, A.
630   Linder, X. Liu, M. Madhavan, R. Makinson, J. Mellors, A. Minassian, M. Moore, Y.
631   Mujadidi, E. Plested, I. Poulton, M. N. Ramasamy, H. Robinson, C. S. Rollier, R. Song,
632   M. D. Snape, R. Tarrant, S. Taylor, K. M. Thomas, M. Voysey, M. E. E. Watson, D.
633   Wright, A. D. Douglas, C. M. Green, A. V. S. Hill, T. Lambe, S. Gilbert, A. J. Pollard, C.
634   V. T. G. Oxford, Phase 1/2 trial of SARS-CoV-2 vaccine ChAdOx1 nCoV-19 with a
635   booster dose induces multifunctional antibody responses. *Nat Med* **27**, 279-288 (2021).
636   8.   J. Grein, N. Ohmagari, D. Shin, G. Diaz, E. Asperges, A. Castagna, T. Feldt, G. Green,
637   M. L. Green, F. X. Lescure, E. Nicastri, R. Oda, K. Yo, E. Quiros-Roldan, A.
638   Studemeister, J. Redinski, S. Ahmed, J. Bernett, D. Chelliah, D. Chen, S. Chihara, S. H.
639   Cohen, J. Cunningham, A. D'Arminio Monforte, S. Ismail, H. Kato, G. Lapadula, E.
640   L'Her, T. Maeno, S. Majumder, M. Massari, M. Mora-Rillo, Y. Mutoh, D. Nguyen, E.
641   Verweij, A. Zoufaly, A. O. Osinusi, A. DeZure, Y. Zhao, L. Zhong, A. Chokkalingam, E.
642   Elboudwarej, L. Telep, L. Timbs, I. Henne, S. Sellers, H. Cao, S. K. Tan, L.
643   Winterbourne, P. Desai, R. Mera, A. Gaggar, R. P. Myers, D. M. Brainard, R. Childs, T.
644   Flanigan, Compassionate Use of Remdesivir for Patients with Severe Covid-19. *N Engl J*
645   *Med* **382**, 2327-2336 (2020).

646   9.   J. H. Beigel, K. M. Tomashek, L. E. Dodd, A. K. Mehta, B. S. Zingman, A. C. Kalil, E.
647   Hohmann, H. Y. Chu, A. Luetkemeyer, S. Kline, D. Lopez de Castilla, R. W. Finberg, K.
648   Dierberg, V. Tapson, L. Hsieh, T. F. Patterson, R. Paredes, D. A. Sweeney, W. R. Short,
649   G. Touloumi, D. C. Lye, N. Ohmagari, M. D. Oh, G. M. Ruiz-Palacios, T. Benfield, G.
650   Fatkenheuer, M. G. Kortepeter, R. L. Atmar, C. B. Creech, J. Lundgren, A. G. Babiker,
651   S. Pett, J. D. Neaton, T. H. Burgess, T. Bonnett, M. Green, M. Makowski, A. Osinusi, S.
652   Nayak, H. C. Lane, A.-S. G. Members, Remdesivir for the Treatment of Covid-19 - Final
653   Report. *N Engl J Med* **383**, 1813-1826 (2020).
654   10.   D. F. Robbiani, C. Gaebler, F. Muecksch, J. C. C. Lorenzi, Z. Wang, A. Cho, M.
655   Agudelo, C. O. Barnes, A. Gazumyan, S. Finkin, T. Hagglof, T. Y. Oliveira, C. Viant, A.
656   Hurley, H. H. Hoffmann, K. G. Millard, R. G. Kost, M. Cipolla, K. Gordon, F. Bianchini,
657   S. T. Chen, V. Ramos, R. Patel, J. Dizon, I. Shimeliovich, P. Mendoza, H. Hartweger, L.
658   Nogueira, M. Pack, J. Horowitz, F. Schmidt, Y. Weisblum, E. Michailidis, A. W.
659   Ashbrook, E. Waltari, J. E. Pak, K. E. Huey-Tubman, N. Koranda, P. R. Hoffman, A. P.
660   West, Jr., C. M. Rice, T. Hatziioannou, P. J. Bjorkman, P. D. Bieniasz, M. Caskey, M. C.
661   Nussenzweig, Convergent antibody responses to SARS-CoV-2 in convalescent
662   individuals. *Nature* **584**, 437-442 (2020).
663   11.   S. J. Zost, P. Gilchuk, R. E. Chen, J. B. Case, J. X. Reidy, A. Trivette, R. S. Nargi, R. E.
664   Sutton, N. Suryadevara, E. C. Chen, E. Binshtein, S. Shrihari, M. Ostrowski, H. Y. Chu,
665   J. E. Didier, K. W. MacRenaris, T. Jones, S. Day, L. Myers, F. Eun-Hyung Lee, D. C.
666   Nguyen, I. Sanz, D. R. Martinez, P. W. Rothlauf, L. M. Bloyet, S. P. J. Whelan, R. S.
667   Baric, L. B. Thackray, M. S. Diamond, R. H. Carnahan, J. E. Crowe, Jr., Rapid isolation
668   and profiling of a diverse panel of human monoclonal antibodies targeting the SARS-
669   CoV-2 spike protein. *Nat Med* **26**, 1422-1427 (2020).
670   12.   D. Pinto, Y. J. Park, M. Beltramello, A. C. Walls, M. A. Tortorici, S. Bianchi, S. Jaconi,
671   K. Culap, F. Zatta, A. De Marco, A. Peter, B. Guarino, R. Spreafico, E. Cameroni, J. B.
672   Case, R. E. Chen, C. Havenar-Daughton, G. Snell, A. Telenti, H. W. Virgin, A.
673   Lanzavecchia, M. S. Diamond, K. Fink, D. Veesler, D. Corti, Cross-neutralization of
674   SARS-CoV-2 by a human monoclonal SARS-CoV antibody. *Nature* **583**, 290-295
675   (2020).
676   13.   A.-T. L.-C. S. Group, J. D. Lundgren, B. Grund, C. E. Barkauskas, T. L. Holland, R. L.
677   Gottlieb, U. Sandkovsky, S. M. Brown, K. U. Knowlton, W. H. Self, D. C. Files, M. K.
678   Jain, T. Benfield, M. E. Bowdish, B. G. Leshnower, J. V. Baker, J. U. Jensen, E. M.
679   Gardner, A. A. Ginde, E. S. Harris, I. S. Johansen, N. Markowitz, M. A. Matthay, L.
680   Ostergaard, C. C. Chang, V. J. Davey, A. Goodman, E. S. Higgs, D. D. Murray, T. A.
681   Murray, R. Paredes, M. K. B. Parmar, A. N. Phillips, C. Reilly, S. Sharma, R. L. Dewar,
682   M. Teitelbaum, D. Wentworth, H. Cao, P. Klekotka, A. G. Babiker, A. C. Gelijns, V. L.
683   Kan, M. N. Polizzotto, B. T. Thompson, H. C. Lane, J. D. Neaton, A Neutralizing
684   Monoclonal Antibody for Hospitalized Patients with Covid-19. *N Engl J Med* **384**, 905-
685   914 (2021).
686   14.   M. P. O'Brien, E. Forleo-Neto, B. J. Musser, F. Isa, K. C. Chan, N. Sarkar, K. J. Bar, R.
687   V. Barnabas, D. H. Barouch, M. S. Cohen, C. B. Hurt, D. R. Burwen, M. A. Marovich, P.
688   Hou, I. Heirman, J. D. Davis, K. C. Turner, D. Ramesh, A. Mahmood, A. T. Hooper, J.
689   D. Hamilton, Y. Kim, L. A. Purcell, A. Baum, C. A. Kyratsous, J. Krainson, R. Perez-
690   Perez, R. Mohseni, B. Kowal, A. T. DiCioccio, N. Stahl, L. Lipsich, N. Braunstein, G.
691   Herman, G. D. Yancopoulos, D. M. Weinreich, T. Covid-19 Phase 3 Prevention Trial,

692   Subcutaneous REGEN-COV Antibody Combination to Prevent Covid-19. *N Engl J Med*,
693   (2021).
694 15. R. E. Chen, X. Zhang, J. B. Case, E. S. Winkler, Y. Liu, L. A. VanBlargan, J. Liu, J. M.
695   Errico, X. Xie, N. Suryadevara, P. Gilchuk, S. J. Zost, S. Tahan, L. Droit, J. S. Turner,
696   W. Kim, A. J. Schmitz, M. Thapa, D. Wang, A. C. M. Boon, R. M. Presti, J. A.
697   O'Halloran, A. H. J. Kim, P. Deepak, D. Pinto, D. H. Fremont, J. E. Crowe, Jr., D. Corti,
698   H. W. Virgin, A. H. Ellebedy, P. Y. Shi, M. S. Diamond, Resistance of SARS-CoV-2
699   variants to neutralization by monoclonal and serum-derived polyclonal antibodies. *Nat*
700   *Med* **27**, 717-726 (2021).
701 16. P. Wang, M. S. Nair, L. Liu, S. Iketani, Y. Luo, Y. Guo, M. Wang, J. Yu, B. Zhang, P. D.
702   Kwong, B. S. Graham, J. R. Mascola, J. Y. Chang, M. T. Yin, M. Sobieszczyk, C. A.
703   Kyratsous, L. Shapiro, Z. Sheng, Y. Huang, D. D. Ho, Antibody resistance of SARS-
704   CoV-2 variants B.1.351 and B.1.1.7. *Nature* **593**, 130-135 (2021).
705 17. D. R. Martinez, A. Schäfer, S. R. Leist, D. Li, K. Gully, B. Yount, J. Y. Feng, E. Bunyan,
706   D. P. Porter, T. Cihlar, S. A. Montgomery, B. F. Haynes, R. S. Baric, M. C.
707   Nussenzweig, T. P. Sheahan, Prevention and therapy of SARS-CoV-2 and the B.1.351
708   variant in mice. *Cell Rep* **36**, 109450 (2021).
709 18. T. P. Sheahan, A. C. Sims, R. L. Graham, V. D. Menachery, L. E. Gralinski, J. B. Case,
710   S. R. Leist, K. Pyrc, J. Y. Feng, I. Trantcheva, R. Bannister, Y. Park, D. Babusis, M. O.
711   Clarke, R. L. Mackman, J. E. Spahn, C. A. Palmiotti, D. Siegel, A. S. Ray, T. Cihlar, R.
712   Jordan, M. R. Denison, R. S. Baric, Broad-spectrum antiviral GS-5734 inhibits both
713   epidemic and zoonotic coronaviruses. *Sci Transl Med* **9**, (2017).
714 19. T. P. Sheahan, A. C. Sims, S. R. Leist, A. Schafer, J. Won, A. J. Brown, S. A.
715   Montgomery, A. Hogg, D. Babusis, M. O. Clarke, J. E. Spahn, L. Bauer, S. Sellers, D.
716   Porter, J. Y. Feng, T. Cihlar, R. Jordan, M. R. Denison, R. S. Baric, Comparative
717   therapeutic efficacy of remdesivir and combination lopinavir, ritonavir, and interferon
718   beta against MERS-CoV. *Nat Commun* **11**, 222 (2020).
719 20. T. P. Sheahan, A. C. Sims, S. Zhou, R. L. Graham, A. J. Pruijssers, M. L. Agostini, S. R.
720   Leist, A. Schafer, K. H. Dinnon, 3rd, L. J. Stevens, J. D. Chappell, X. Lu, T. M. Hughes,
721   A. S. George, C. S. Hill, S. A. Montgomery, A. J. Brown, G. R. Bluemling, M. G.
722   Natchus, M. Saindane, A. A. Kolykhalov, G. Painter, J. Harcourt, A. Tamin, N. J.
723   Thornburg, R. Swanstrom, M. R. Denison, R. S. Baric, An orally bioavailable broad-
724   spectrum antiviral inhibits SARS-CoV-2 in human airway epithelial cell cultures and
725   multiple coronaviruses in mice. *Sci Transl Med* **12**, (2020).
726 21. A. Wahl, L. E. Gralinski, C. E. Johnson, W. Yao, M. Kovarova, K. H. Dinnon, 3rd, H.
727   Liu, V. J. Madden, H. M. Krzystek, C. De, K. K. White, K. Gully, A. Schafer, T. Zaman,
728   S. R. Leist, P. O. Grant, G. R. Bluemling, A. A. Kolykhalov, M. G. Natchus, F. B. Askin,
729   G. Painter, E. P. Browne, C. D. Jones, R. J. Pickles, R. S. Baric, J. V. Garcia, SARS-
730   CoV-2 infection is effectively treated and prevented by EIDD-2801. *Nature* **591**, 451-457
731   (2021).
732 22. W. Fischer, J. J. Eron, W. Holman, M. S. Cohen, L. Fang, L. J. Szewczyk, T. P. Sheahan,
733   R. Baric, K. R. Mollan, C. R. Wolfe, E. R. Duke, M. M. Azizad, K. Borroto-Esoda, D. A.
734   Wohl, A. J. Loftis, P. Alabanza, F. Lipansky, W. P. Painter, Molnupiravir, an Oral
735   Antiviral Treatment for COVID-19. *medRxiv*, (2021).
736 23. B. N. Williamson, F. Feldmann, B. Schwarz, K. Meade-White, D. P. Porter, J. Schulz, N.
737   van Doremalen, I. Leighton, C. Kwe Yinda, L. Perez-Perez, A. Okumura, J. Lovaglio, P.
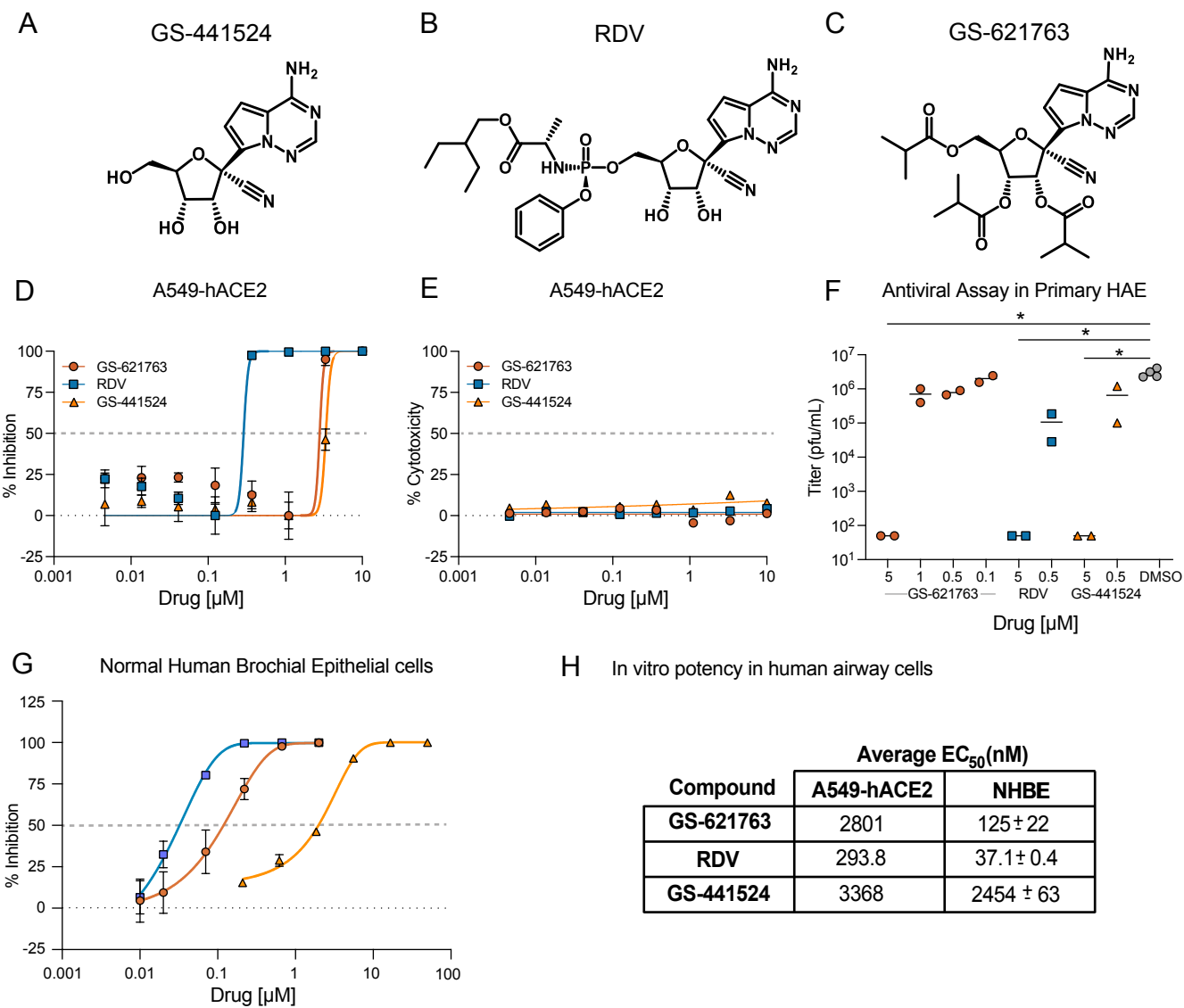
738   W. Hanley, G. Saturday, C. M. Bosio, S. Anzick, K. Barbian, T. Cihlar, C. Martens, D. P.
739   Scott, V. J. Munster, E. de Wit, Clinical benefit of remdesivir in rhesus macaques
740   infected with SARS-CoV-2. *bioRxiv*, (2020).
741 24. D. R. Owen, C. M. N. Allerton, A. S. Anderson, L. Aschenbrenner, M. Avery, S. Berritt,
742   B. Boras, R. D. Cardin, A. Carlo, K. J. Coffman, A. Dantonio, L. Di, H. Eng, R. Ferre, K.
743   S. Gajiwala, S. A. Gibson, S. E. Greasley, B. L. Hurst, E. P. Kadar, A. S. Kalgutkar, J. C.
744   Lee, J. Lee, W. Liu, S. W. Mason, S. Noell, J. J. Novak, R. S. Obach, K. Ogilvie, N. C.
745   Patel, M. Pettersson, D. K. Rai, M. R. Reese, M. F. Sammons, J. G. Sathish, R. S. P.
746   Singh, C. M. Steppan, A. E. Stewart, J. B. Tuttle, L. Updyke, P. R. Verhoest, L. Wei, Q.
747   Yang, Y. Zhu, An Oral SARS-CoV-2 M^{pro} Inhibitor Clinical Candidate for
748   the Treatment of COVID-19. *medRxiv*, 2021.2007.2028.21261232 (2021).
749 25. S. S. Good, J. Westover, K. H. Jung, X. J. Zhou, A. Moussa, P. La Colla, G. Collu, B.
750   Canard, J. P. Sommadossi, AT-527, a Double Prodrug of a Guanosine Nucleotide
751   Analog, Is a Potent Inhibitor of SARS-CoV-2 In Vitro and a Promising Oral Antiviral for
752   Treatment of COVID-19. *Antimicrob Agents Chemother* **65**, (2021).
753 26. A. J. Pruijssers, A. S. George, A. Schafer, S. R. Leist, L. E. Gralinksi, K. H. Dinnon, 3rd,
754   B. L. Yount, M. L. Agostini, L. J. Stevens, J. D. Chappell, X. Lu, T. M. Hughes, K.
755   Gully, D. R. Martinez, A. J. Brown, R. L. Graham, J. K. Perry, V. Du Pont, J. Pitts, B.
756   Ma, D. Babusis, E. Murakami, J. Y. Feng, J. P. Bilello, D. P. Porter, T. Cihlar, R. S.
757   Baric, M. R. Denison, T. P. Sheahan, Remdesivir Inhibits SARS-CoV-2 in Human Lung
758   Cells and Chimeric SARS-CoV Expressing the SARS-CoV-2 RNA Polymerase in Mice.
759   *Cell Rep* **32**, 107940 (2020).
760 27. R. L. Mackman, H. C. Hui, M. Perron, E. Murakami, C. Palmiotti, G. Lee, K. Stray, L.
761   Zhang, B. Goyal, K. Chun, D. Byun, D. Siegel, S. Simonovich, V. Du Pont, J. Pitts, D.
762   Babusis, A. Vijjapurapu, X. Lu, C. Kim, X. Zhao, J. Chan, B. Ma, D. Lye, A.
763   Vandersteen, S. Wortman, K. T. Barrett, M. Toteva, R. Jordan, R. Subramanian, J. P.
764   Bilello, T. Cihlar, Prodrugs of a 1'-CN-4-Aza-7,9-dideazaadenosine C-Nucleoside
765   Leading to the Discovery of Remdesivir (GS-5734) as a Potent Inhibitor of Respiratory
766   Syncytial Virus with Efficacy in the African Green Monkey Model of RSV. *J Med Chem*
767   **64**, 5001-5017 (2021).
768 28. Y. J. Hou, K. Okuda, C. E. Edwards, D. R. Martinez, T. Asakura, K. H. Dinnon, 3rd, T.
769   Kato, R. E. Lee, B. L. Yount, T. M. Mascenik, G. Chen, K. N. Olivier, A. Ghio, L. V.
770   Tse, S. R. Leist, L. E. Gralinski, A. Schafer, H. Dang, R. Gilmore, S. Nakano, L. Sun, M.
771   L. Fulcher, A. Livraghi-Butrico, N. I. Nicely, M. Cameron, C. Cameron, D. J. Kelvin, A.
772   de Silva, D. M. Margolis, A. Markmann, L. Bartelt, R. Zumwalt, F. J. Martinez, S. P.
773   Salvatore, A. Borczuk, P. R. Tata, V. Sontake, A. Kimple, I. Jaspers, W. K. O'Neal, S. H.
774   Randell, R. C. Boucher, R. S. Baric, SARS-CoV-2 Reverse Genetics Reveals a Variable
775   Infection Gradient in the Respiratory Tract. *Cell* **182**, 429-446 e414 (2020).
776 29. X. Xie, A. E. Muruato, X. Zhang, K. G. Lokugamage, C. R. Fontes-Garfias, J. Zou, J.
777   Liu, P. Ren, M. Balakrishnan, T. Cihlar, C. K. Tseng, S. Makino, V. D. Menachery, J. P.
778   Bilello, P. Y. Shi, A nanoluciferase SARS-CoV-2 for rapid neutralization testing and
779   screening of anti-infective drugs for COVID-19. *Nat Commun* **11**, 5214 (2020).
780 30. S. R. Leist, K. H. Dinnon, 3rd, A. Schäfer, L. V. Tse, K. Okuda, Y. J. Hou, A. West, C.
781   E. Edwards, W. Sanders, E. J. Fritch, K. L. Gully, T. Scobey, A. J. Brown, T. P. Sheahan,
782   N. J. Moorman, R. C. Boucher, L. E. Gralinski, S. A. Montgomery, R. S. Baric, A

783   Mouse-Adapted SARS-CoV-2 Induces Acute Lung Injury and Mortality in Standard
784   Laboratory Mice. *Cell* **183**, 1070-1085.e1012 (2020).
785   31. R. L. Graham, E. F. Donaldson, R. S. Baric, A decade after SARS: strategies for
786   controlling emerging coronaviruses. *Nat Rev Microbiol* **11**, 836-848 (2013).
787   32. L. Rosenbaum, Escaping Catch-22 - Overcoming Covid Vaccine Hesitancy. *N Engl J
788   Med* **384**, 1367-1371 (2021).
789   33. B. Adhikari, P. Y. Cheah, Vaccine hesitancy in the COVID-19 era. *Lancet Infect Dis*,
790   (2021).
791   34. Z. Wang, F. Schmidt, Y. Weisblum, F. Muecksch, C. O. Barnes, S. Finkin, D. Schaefer-
792   Babajew, M. Cipolla, C. Gaebler, J. A. Lieberman, T. Y. Oliveira, Z. Yang, M. E.
793   Abernathy, K. E. Huey-Tubman, A. Hurley, M. Turroja, K. A. West, K. Gordon, K. G.
794   Millard, V. Ramos, J. Da Silva, J. Xu, R. A. Colbert, R. Patel, J. Dizon, C. Unson-
795   O'Brien, I. Shimeliovich, A. Gazumyan, M. Caskey, P. J. Bjorkman, R. Casellas, T.
796   Hatziioannou, P. D. Bieniasz, M. C. Nussenzweig, mRNA vaccine-elicited antibodies to
797   SARS-CoV-2 and circulating variants. *Nature* **592**, 616-622 (2021).
798   35. A. J. Brown, J. J. Won, R. L. Graham, K. H. Dinnon, 3rd, A. C. Sims, J. Y. Feng, T.
799   Cihlar, M. R. Denison, R. S. Baric, T. P. Sheahan, Broad spectrum antiviral remdesivir
800   inhibits human endemic and zoonotic deltacoronaviruses with a highly divergent RNA
801   dependent RNA polymerase. *Antiviral Res* **169**, 104541 (2019).
802   36. W. T. Harvey, A. M. Carabelli, B. Jackson, R. K. Gupta, E. C. Thomson, E. M. Harrison,
803   C. Ludden, R. Reeve, A. Rambaut, C.-G. U. Consortium, S. J. Peacock, D. L. Robertson,
804   SARS-CoV-2 variants, spike mutations and immune escape. *Nat Rev Microbiol* **19**, 409-
805   424 (2021).
806   37. D. C. Montefiori, P. Acharya, SnapShot: SARS-CoV-2 antibodies. *Cell Host Microbe* **29**,
807   1162-1162 e1161 (2021).
808   38. R. Martin, J. Li, A. Parvangada, J. Perry, T. Cihlar, H. Mo, D. Porter, E. Svarovskaia,
809   Genetic conservation of SARS-CoV-2 RNA replication complex in globally circulating
810   isolates and recently emerged variants from humans and minks suggests minimal pre-
811   existing resistance to remdesivir. *Antiviral Res* **188**, 105033 (2021).
812   39. Y. Liu, L. M. Yan, L. Wan, T. X. Xiang, A. Le, J. M. Liu, M. Peiris, L. L. M. Poon, W.
813   Zhang, Viral dynamics in mild and severe cases of COVID-19. *Lancet Infect Dis* **20**, 656-
814   657 (2020).
815   40. S. Zheng, J. Fan, F. Yu, B. Feng, B. Lou, Q. Zou, G. Xie, S. Lin, R. Wang, X. Yang, W.
816   Chen, Q. Wang, D. Zhang, Y. Liu, R. Gong, Z. Ma, S. Lu, Y. Xiao, Y. Gu, J. Zhang, H.
817   Yao, K. Xu, X. Lu, G. Wei, J. Zhou, Q. Fang, H. Cai, Y. Qiu, J. Sheng, Y. Chen, T.
818   Liang, Viral load dynamics and disease severity in patients infected with SARS-CoV-2 in
819   Zhejiang province, China, January-March 2020: retrospective cohort study. *BMJ* **369**,
820   m1443 (2020).
821   41. F. Zhou, T. Yu, R. Du, G. Fan, Y. Liu, Z. Liu, J. Xiang, Y. Wang, B. Song, X. Gu, L.
822   Guan, Y. Wei, H. Li, X. Wu, J. Xu, S. Tu, Y. Zhang, H. Chen, B. Cao, Clinical course
823   and risk factors for mortality of adult inpatients with COVID-19 in Wuhan, China: a
824   retrospective cohort study. *Lancet* **395**, 1054-1062 (2020).
825   42. X. Lu, L. Wang, S. K. Sakthivel, B. Whitaker, J. Murray, S. Kamili, B. Lynch, L.
826   Malapati, S. A. Burke, J. Harcourt, A. Tamin, N. J. Thornburg, J. M. Villanueva, S.
827   Lindstrom, US CDC Real-Time Reverse Transcription PCR Panel for Detection of
828   Severe Acute Respiratory Syndrome Coronavirus 2. *Emerg Infect Dis* **26**, (2020).
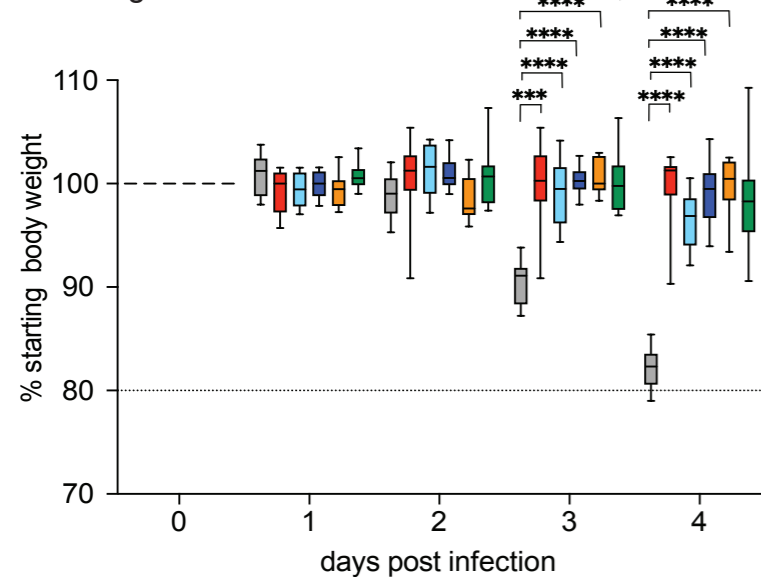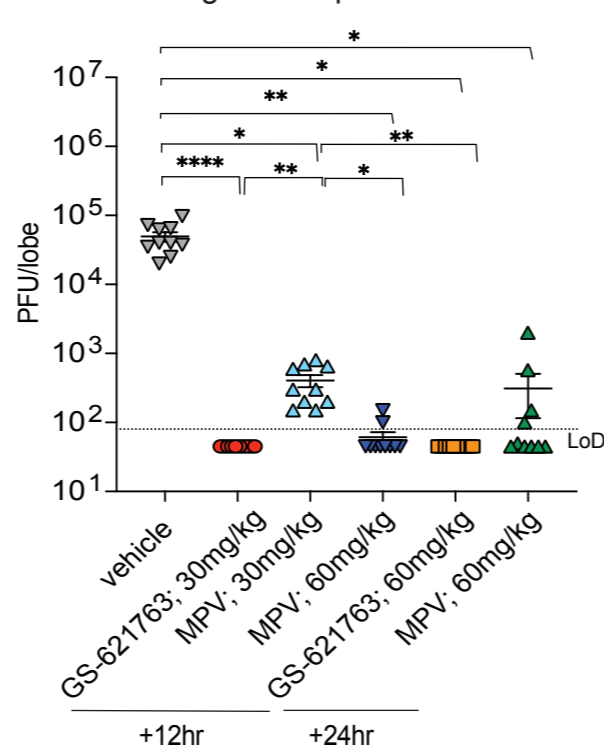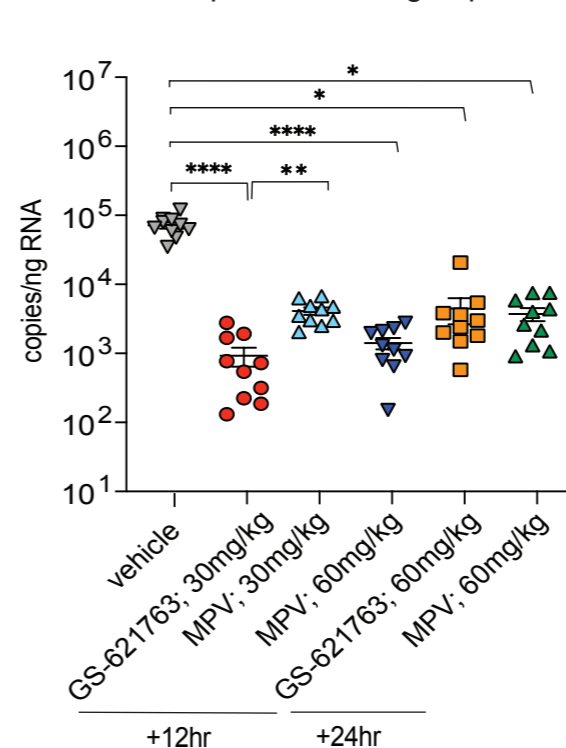
Version 9.4 32

829

Figure 1

A GS-441524

B RDV

C GS-621763

D A549-hACE2

- GS-621763
- RDV
- GS-441524

% Inhibition vs Drug [μM]

E A549-hACE2

- GS-621763
- RDV
- GS-441524

% Cytotoxicity vs Drug [μM]

F Antiviral Assay in Primary HAE

Titer (pfu/mL) vs Drug [μM]

GS-621763: 5, 1, 0.5, 0.1 | RDV: 5, 0.5 | GS-441524: 5, 0.5 | DMSO

G Normal Human Brochial Epithelial cells

% Inhibition vs Drug [μM]

H In vitro potency in human airway cells

	Average EC$_{50}$(nM)	
Compound	**A549-hACE2**	**NHBE**
GS-621763	2801	125 ± 22
RDV	293.8	37.1 ± 0.4
GS-441524	3368	2454 ± 63

Figure 4

A. Weight Loss

B. Viral Lung Titer 4dpi
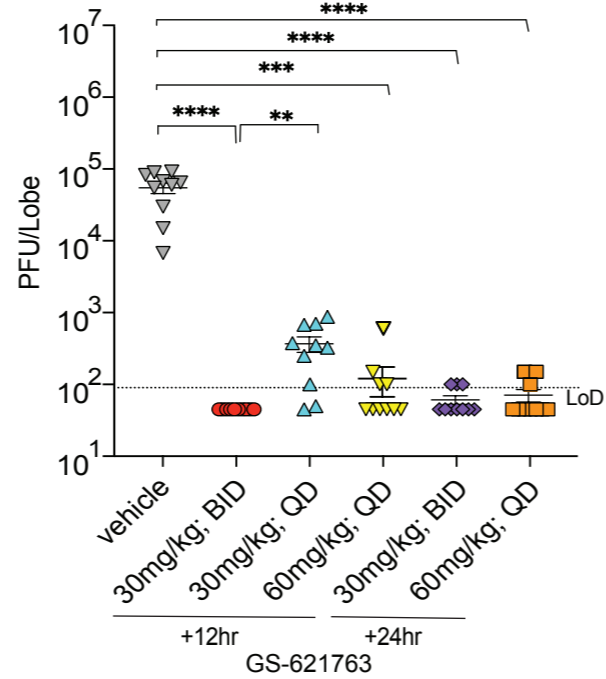
C. Nucleocapsid RNA Lung 4dpi
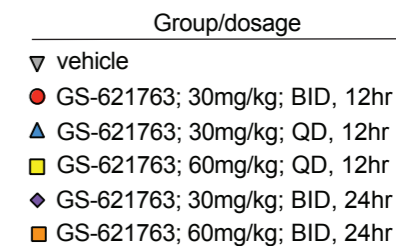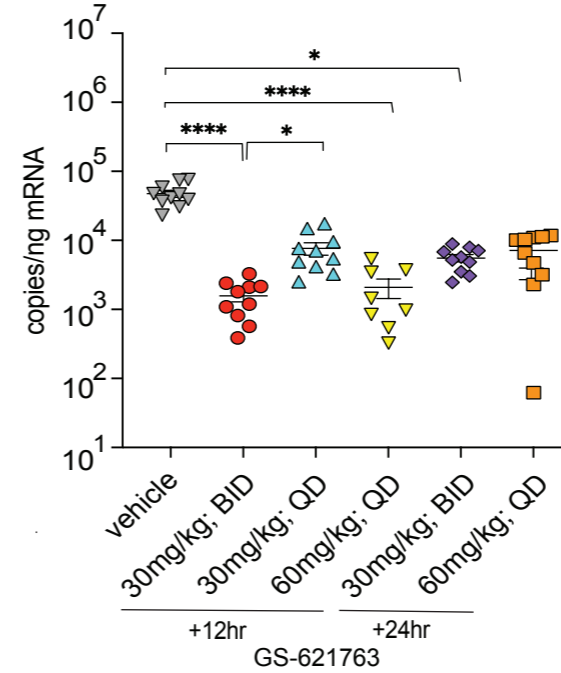
D. Pulmonary Function
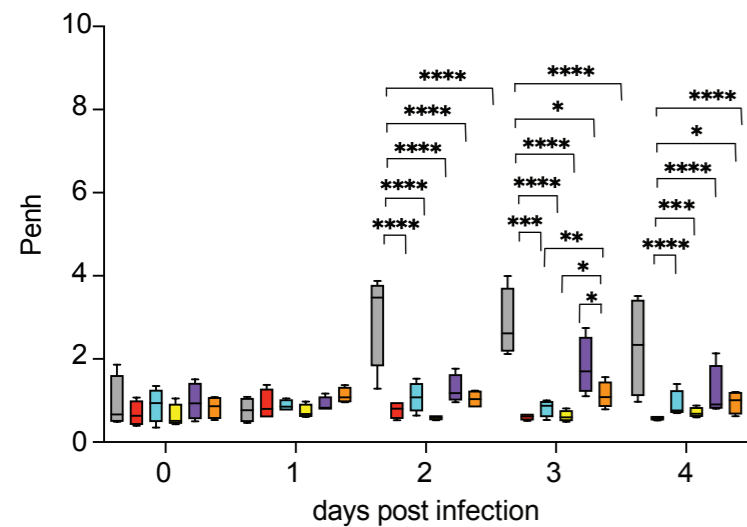
E. ATS Acute Lung Injury 4dpi

F. Diffuse Alveolar Damage 4dpi

Group/dosage

- vehicle
- GS-621763; 30mg/kg BID, 12hr
- MPV; 30mg/kg; BID, 12hr
- MPV; 60mg/kg; BID, 12hr
- GS-621763; 60mg/kg; BID, 24hr
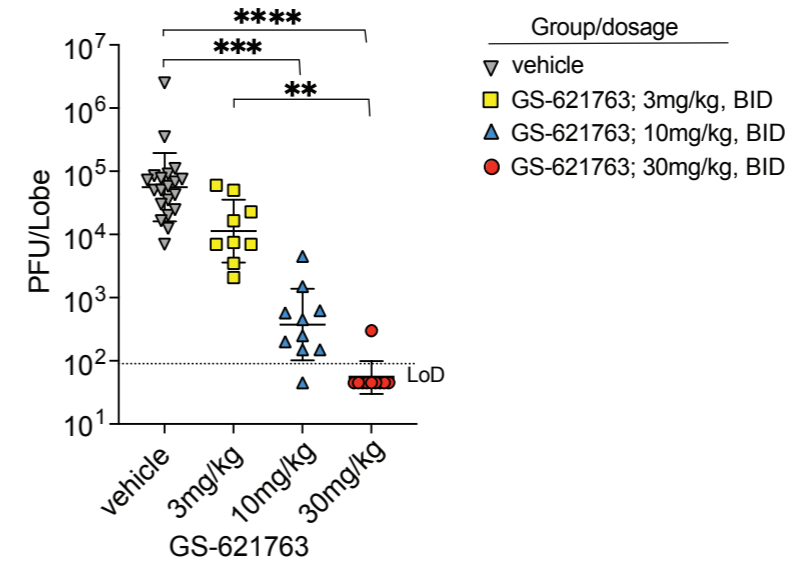- MPV; 60mg/kg; BID, 24hr

Figure 3

Figure 2
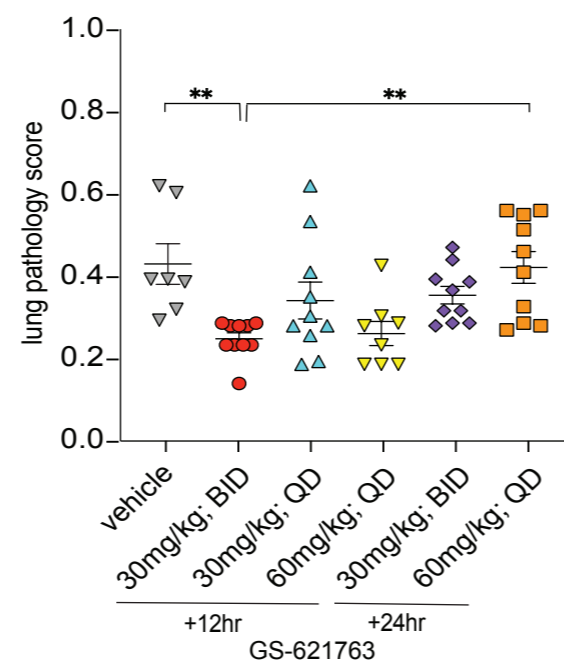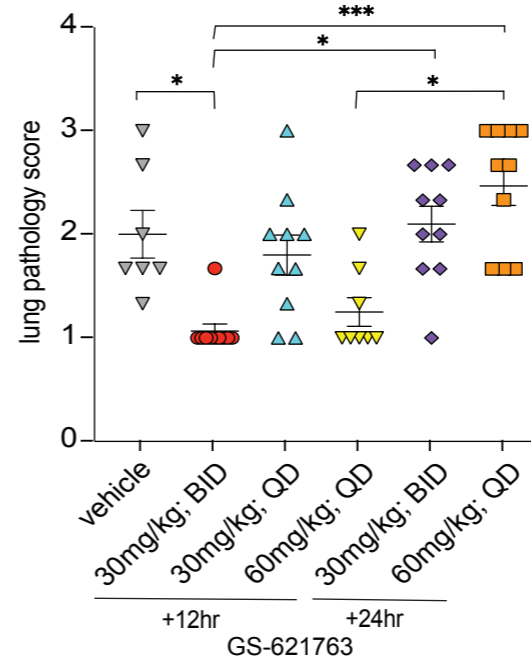
A. Plasma pharmacokinetics
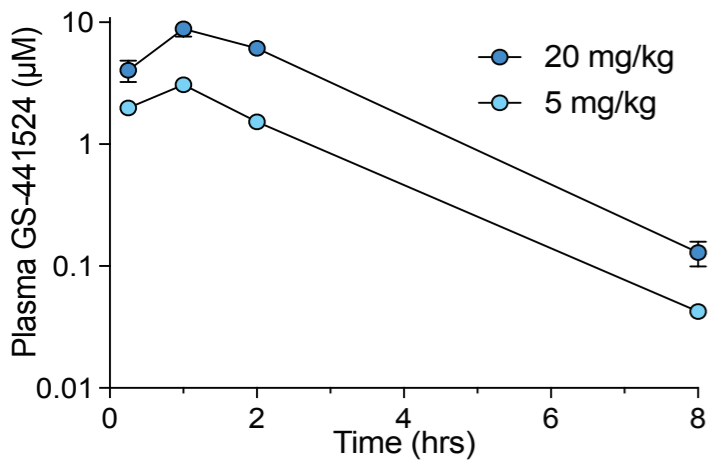
B. Weight loss
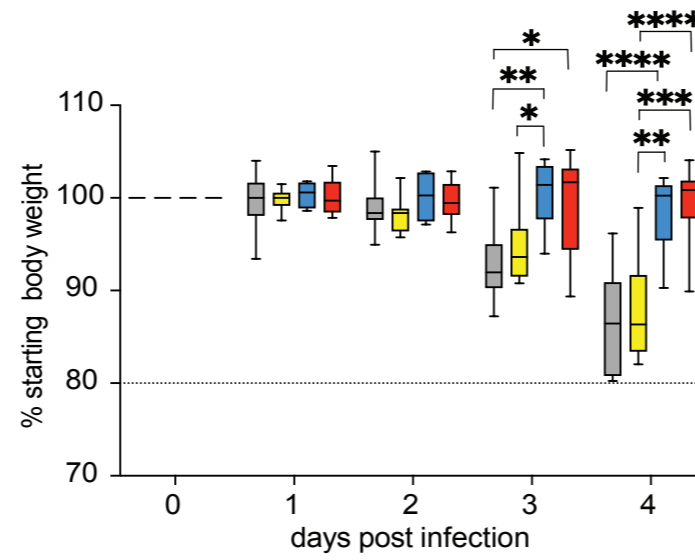
C. Viral Titer Lung 4dpi

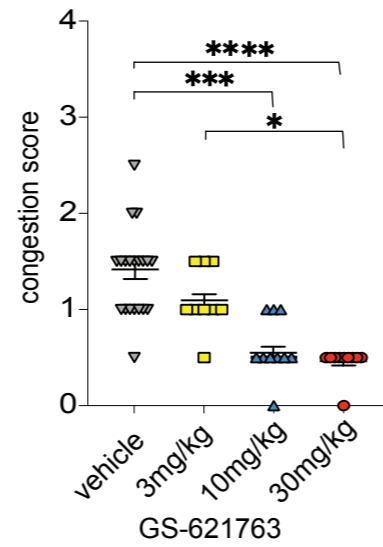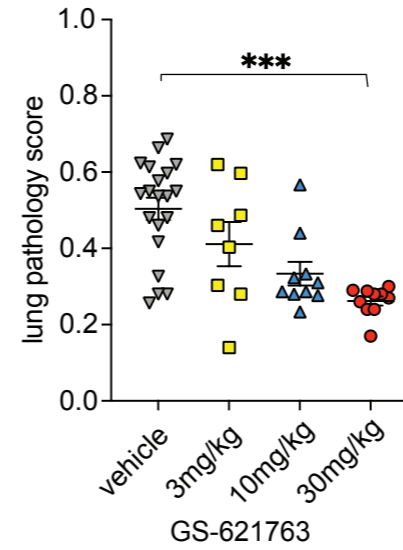**D.** Pulmonary Function
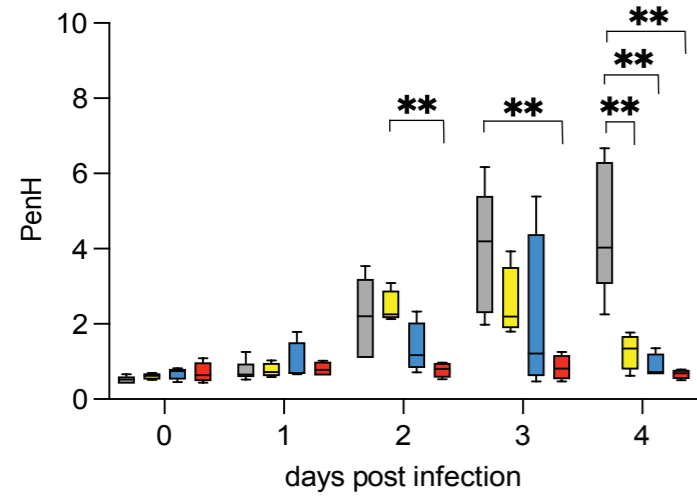
E. Congestion Score 4dpi

F. ATS Acute Lung Injury 4dpi

G. Diffuse Alveolar Damage 4dpi